ICSV 21
13-17 July, 2014, Beijing/China

The 21st International Congress on Sound and Vibration

13-17 July, 2014, Beijing/China

INVESTIGATION OF AIRFOIL TRAILING EDGE NOISE WITH ADVANCED EXPERIMENTAL AND NUMERICAL METHODS

Tom Gerhard and Thomas Carolus

Institute for Fluid- and Thermodynamics, University of Siegen, Siegen, Germany

e-mail: tom.gerhard@uni-siegen.de

The investigation of the noise emitted from the trailing edge (TE) of a Somers S834 airfoil section with advanced experimental and numerical methods is presented. The airfoil section is placed in a low noise, low turbulence small aeroacoustic wind tunnel. To mimic a relatively large target Reynolds number the boundary layer on the airfoil has to be tripped. An unsteady large-eddy simulation (LES) provides the input data for airfoil self noise prediction models. Standard microphone correlation as well as microphone array based techniques were applied to distinguish trailing edge noise (TEN) from ambient sound and for quantification.
The carefully applied boundary layer tripping produced the targeted boundary layer parameters in the TE region of the airfoil. The TE of the airfoil was found to be the most dominant sound radiation region on the airfoil section. The microphone array measurements revealed dominant contributions from the TE from 160 to at least 2500 Hz. The peak level of TEN was found at a displacement thickness based Strouhal-number of approximately 0.075, corresponding to a frequency of 500 Hz. Both sound prediction models utilized - Brooks, Pope and Marcolini (BPM) and Curle's - confirmed that the spectral hump found in the measurements is indeed attributed to the turbulent flow over the airfoil's trailing edge.

1. Introduction

The growing impact of turbo-machinery applications on public life results in stricter noise regulations. Key topics of actual research activities are aero-acoustically generated sound e.g. from aircraft engines or onshore wind turbines. The interaction of the flow with the aerodynamically effective surfaces, e.g. the rotor blade, is responsible for various sound sources. Brooks, Pope and Marcolini[1] attributed the sound from an airfoil section subject to a flow to five main mechanisms, (i) separation-stall, (ii) tip vortex formation, (iii) trailing-edge-bluntness vortex-shedding, (iv) laminar-boundary-layer vortex-shedding and (v) turbulent-boundary-layer trailing-edge (TBL-TE). According to Roger[2], the scattering of the turbulent boundary layer at the airfoil TE acts as the dominant sound source of airfoils in a temporally and spatially homogeneous flow. In general sound or noise from trailing edges is called trailing edge noise (TEN).

The overall target of our current research is studying TEN and possible mitigation measures. This paper is focussing on the experimental and numerical investigation of the acoustic emissions from airfoils. As a generic example we consider a two-dimensional S834 airfoil section employed in wind turbine technology. This airfoil shape has been developed by Somers[3] and was originally designed for small and quiet horizontal axis wind turbines. Oerlemans[4] investigated the acoustic properties of the S834 airfoil in an aeroacoustic wind tunnel by means of microphone array meas-

urements using the conventional sum-and-delay beam forming algorithm. For tripped conditions he indeed found the airfoil TE to be the most efficient sound emitting part. This was encouraging for this study considering the flow and sound generating mechanisms in the TE region in more detail. Since we target at larger wind turbines, the Reynolds number and the associated boundary layer parameters must be appropriate

As compared to experimental techniques, numerical approaches offer the advantage of closing the gap between the unsteady, physical flow field and the sound radiated. Numerous studies are known, dealing with the unsteady turbulent flow field around airfoils or turbomachinery rotors and the subsequent calculation of the sound field by acoustic analogies or computational aeroacoustic methods. Winkler et al.[5] performed a large eddy simulation (LES) of the flow around an airfoil section, used the data as input to various acoustic models and found satisfactory agreement between sound prediction and experimental results. In the present study tripping is not only done for the experiments but is also taken into account in the numerical flow simulation.

2. Methodology

2.1 Airfoil Section and Test Rig

The investigated S834 airfoil section has a chord length of c = 0.2 m and an aspect ratio of 1.33, Fig. 1 (right). The angle of attack (AOA) is chosen such that an infinite aspect ratio section of this airfoil would operate at its optimal lift to drag ratio for a chord based Reynolds number Re = $3.5 \cdot 10^6$. This requires an effective AOA $\alpha_{eff} = 4.7°$.

The airfoil section is mounted between sideplates in an open wind tunnel, $0.5 \cdot c$ downstream of the nozzle exit, Fig. 1 (left). To compensate for open wind tunnel installation effects, a correction as derived by Brooks et al.[6] is applied, leading to a geometric AOA of $\alpha_{geom} = 12.7°$ for this particular aspect ratio.

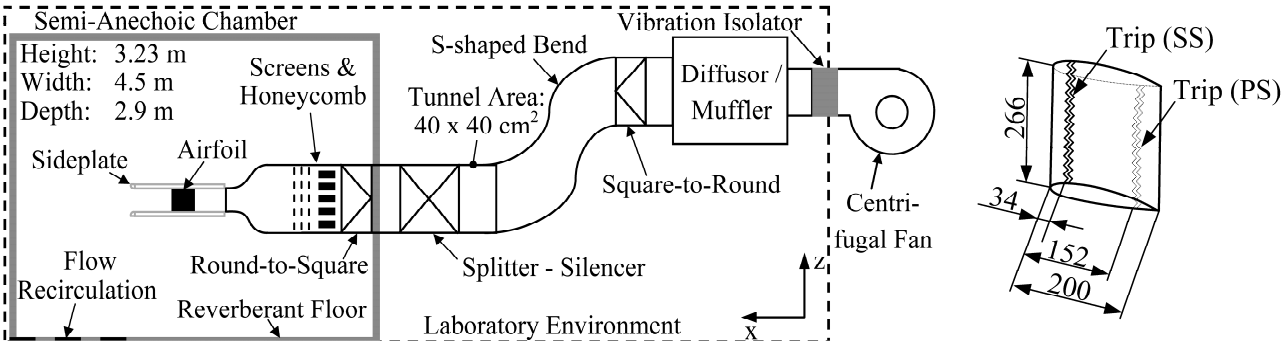

Figure 1. Left: Schematic layout of the small aeroacoustic wind tunnel at the University of Siegen (not to scale); right: Sketch of the S834 airfoil section with trip positions (dimensions in mm, not to scale)

The available small aeroacoustic wind tunnel provides a maximum flow velocity resulting only in $Re = 3.5 \cdot 10^5$. To mimic the 10-times higher target Reynolds number the location of boundary layer transition on both, pressure and suction side (SS) of the airfoil section were controlled by a zigzag tape. The tripping locations were selected such that they correspond to the chordwise location of natural transition for the S834 airfoil at the target Reynolds number. The locations of natural transition were found via the airfoil performance prediction tool XFOIL[7]. XFOIL yields overall airfoil characteristics like lift and drag coefficients as a function of airfoil shape, AOA, Reynolds and Mach number in an undisturbed flow (i.e. without any effect of an open wind tunnel). Since it is based on a linear-vorticity second order accurate panel method coupled with an integral boundary layer method and an e^n-type transition amplification formulation[8], it also allows a prediction of the transition locations. For our case transition must occur at x/c = 0.17 on the airfoil suction and x/c = 0.76 on the pressure side, hence the zigzag tape is applied at exactly these chordwise positions along the complete span. All investigations were carried out at a Mach-number of M = 0.075.

The time-averaged chordwise pressure distribution from leading to trailing edge was measured via 31 pinholes connected by tubes to a 16 channel pressure transducer (Pressure Systems Inc., type PSI 9116). It allowed a synchronous measuring of the complete pressure distribution at either side of the airfoil. Since the surface pressure fluctuations in the trailing edge region were of special interest, the airfoil was instrumented with nine flush mounted miniature pressure transducers (Knowles Acoustics, type FG-3329-P07) as documented in Fig. 2. This arrangement of sensors allowed the synchronous determination of the stream- and spanwise unsteady pressure field in the airfoil TE region. Basically these transducers are miniature condenser microphones with a sensitive diameter of 0.7 mm. They have been calibrated in-situ with a white noise excitation signal ranging from 100 Hz to 10 kHz. Flow velocity and turbulence parameters in the airfoil boundary layer were measured with a 1-D hot-wire anemometer (TSI™, type: 1210-T1.5). The 1.25 mm long wire is made of tungsten and has a diameter of 5 µm. The probe is operating in a constant-temperature mode using the Streamline™ unit from Dantec Dynamics. For the exact positioning of the probe a three-axes traverse system was used.

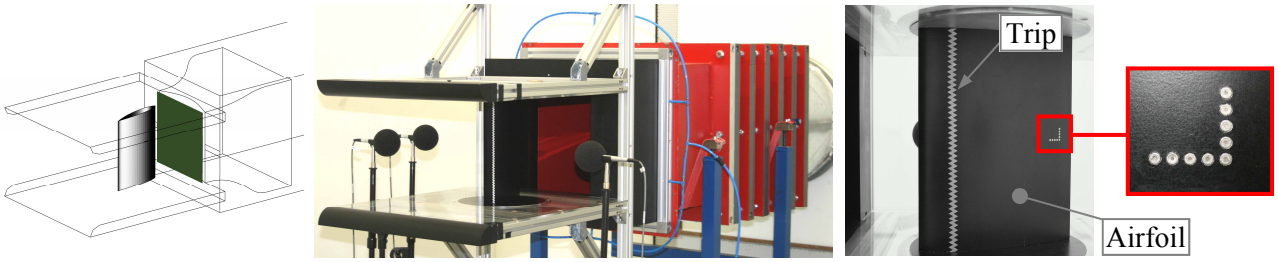

Figure 2. Left: Sketch of the test rig; middle: Airfoil section between side plates attached to wind tunnel nozzle; right: field of miniature pressure transducers in the trailing edge region.

The wind tunnel (for details see Winkler and Carolus[9]) exhausts in a semi-anechoic chamber (4.5 m x 3.23 m x 2.9 m) which allows acoustic measurements according to ISO 3745[10] down to 125 Hz. The characteristic turbulence intensity in a plane 0.01 m downstream of the wind tunnel nozzle exit is 0.2 %. The sound from the airfoil section is measured synchronously by three microphones (1/2" Brüel & Kjaer™, type 4190), each located outside of the jet in a distance of 0.3 m from the center line, Fig. 3 (left). The microphones are equipped with a wind screen to avoid any flow induced pseudo sound. In addition to this local sound pressure measurement technique a microphone array (CAE Noise Inspector™) was utilized. The array consists of 40 condenser microphones which are spread over a plane area of 0.5 m^2, Fig. 3 (right).

2.2 Acoustic Signal Processing Techniques

The acoustic signature from the airfoil is relatively low level and potentially contaminated by extraneous sound sources. Three different techniques are applied for isolation of TEN.

Firstly we take advantage of the fact that the TE essentially is a dipole sound source. Hence a filtering technique derived by Blake and Lynch[11] is applied using the cross-correlation of two phase-matched TE microphones (here M2 and M3, Fig. 3 left). Because of the dipole directivity pattern the signals of both microphones should be equal in magnitude but 180° out of phase. The preparatory work is done by a first filter that removes all frequency components for which the level of the cross-spectral density (CSD) is less the 6 dB above the background CSD level. The second filter rejects all frequencies where the phase shift of the CSD is not within a range of 180°±9°. Upon applying both filters, the spectrum contains theoretically only pure TEN. The drawback of the filtering technique by Blake and Lynch is that sound generated at the airfoil leading edge (LE) due to ingested turbulence, has the same dipole characteristics and could distort the TEN signal.

Secondly, to locate the main dipole sound sources from the airfoil, Brooks Pope and Marcolini[1] developed a simple correlation method utilizing cross-correlation. The wave travelling time due to different distances from source to two microphones (here M2 and M1, Fig. 3 left) allows drawing conclusion on the main source location.

A third technique is based on the array of microphones. For the low frequency range ($f < 600$ Hz) near field holography is applied to localize sound radiating areas on the airfoil. For that the array is positioned 0.25 m next to the airfoil suction side surface. For signals in a frequency band 600 Hz $< f <$ 1200 Hz orthogonal beamforming and for all higher frequencies the Clean SC[12] algorithm is applied (the array is then positioned 0.75 m next to the airfoil suction side surface, Fig. 3 right).

With exception of the microphone array all unsteady quantities were captured with a sampling frequency f_s = 51.2 kHz. The spectral analysis is based on the power spectral density (PSD) obtained by the *pwelch* routine in MATLAB® 2012a (Δf = 1 Hz, $p_0 = 2 \cdot 10^{-5}$ Pa, f_0 = 1 Hz). The sampling rate for all 40 microphones from the microphone array was 48 kHz with 24 bits resolution.

Figure 3. Left: Airfoil section and microphone positions (top view); right: Microphone array next to airfoil

2.3 Numerical Set Up

A steady-state, incompressible 3D Reynolds-averaged Navier-Stokes (RANS) simulation using the standard k-ω-SST turbulence model derived by Menter[13] was performed. The RANS domain includes the anechoic chamber, the sideplates, the complete airfoil and the nozzle. The results of this simulation provide the inflow boundary conditions for the integrated LES domain of a spanwise airfoil section, Fig. 4. The main wind tunnel installation effects were taken into account due to the upstream extension of the LES domain up to the nozzle exit. The LES domain extends $5.75 \cdot c$ in streamwise, $3 \cdot c$ in crosswise and $0.075 \cdot c$ in spanwise direction. At the inlet plane and at the crosswise boundaries the velocities taken from the RANS simulations are used as boundary conditions. In spanwise direction periodic boundary conditions are predefined, the outlet is executed as a pressure outlet. The 3D-block-structured numerical grid of the LES consists of $8.5 \cdot 10^6$ cells, with an averaged local grid spacing of about $\Delta x^+ \approx 70$, $\Delta y^+ \approx 0.4$, $\Delta z^+ \approx 30$. The wall-resolving LES utilizes a wall adaptive local eddy viscosity (WALE) subgrid-scale model by Nicoud and Ducros[14] and a dimensionless time step-size based on freestream velocity and chord length of $\Delta t = 6.4 \cdot 10^{-4}$. The convective Courant-Friedrichs-Lewy number is only locally above 1. The flow solver is based on a finite volume method and 2nd order accurate in space and time. For the time integration a bounded 2nd order implicit spatial scheme is used, the spatial integration is done by a bounded central differencing scheme. The reached convergence criteria of all variables are $1 \cdot 10^{-6}$. The simulation ran for 15 flow-through times. The applied tripping is considered in case of a representative step with the height and an average length of the experimentally used zigzag tape, Fig. 4 (right). The commercial Navier-Stokes code ANSYS FLUENT™ version 14.5 has been used throughout this study.

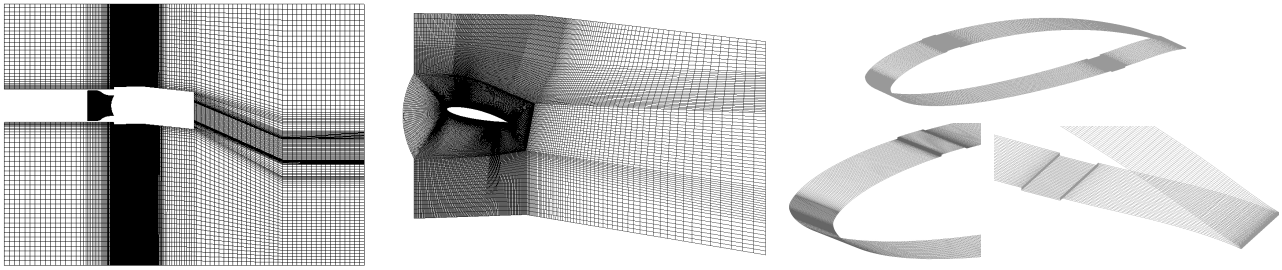

Figure 4. Left: Grid topology of the wind-tunnel setup for initial RANS computations, middle: truncated LES domain, extracted from the full wind-tunnel setup (every 2nd mesh line visible); right: numerical surface grid of the simulated airfoil section with close up view on the airfoil LE and TE with the applied tripping.

3. Results

3.1 Aerodynamic Results

Fig. 5 shows the mean pressure distribution around the airfoil and the boundary layer displacement thickness on the suction side. (The boundary layer displacement, especially at the trailing edge, is an important parameter for TEN prediction models). Note that we compare experimental and numerical results from the tripped airfoil section operating in the small wind tunnel at $Re = 3.5 \cdot 10^5$ and $\alpha_{geom} = 12.7°$ with the XFOIL-prediction of the untripped, at $Re = 3.5 \cdot 10^6$ and with $\alpha_{eff} = 4.7°$ operating airfoil. The results from experiments, RANS and LES, and XFOIL agree quite well. The local pressure peaks occurring for the LES are caused by the tripping which is not included in the RANS simulation.

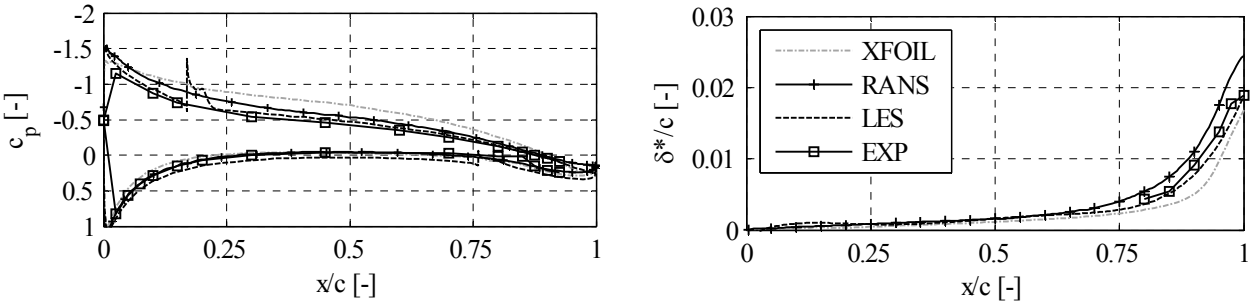

Figure 5. Left: Mean pressure distribution on airfoil surface, right: displacement thickness (SS), $Re = 3.5 \cdot 10^5$ and $\alpha_{geom} = 12.7°$; for comparison: XFOIL results for $Re = 3.5 \cdot 10^6$ and $\alpha_{eff} = 4.7°$.

The LES predicted fluctuating pressure on the airfoil suction side is depicted in Fig. 6 (left). The root-mean-square (rms) values increase at the trip ($x/c = 0.17$) and again slightly at the TE. The dominant frequency parts shift from higher frequencies in the LE region towards lower frequencies at the rear part of the airfoil. Figure 6 (right) shows a comparison of the measured and the LES-predicted surface pressure spectra at $x/c = 0.8$ on the airfoil suction side. The agreement is not perfect, but the numerical prediction shows the tendencies of the experimental spectra quite well.

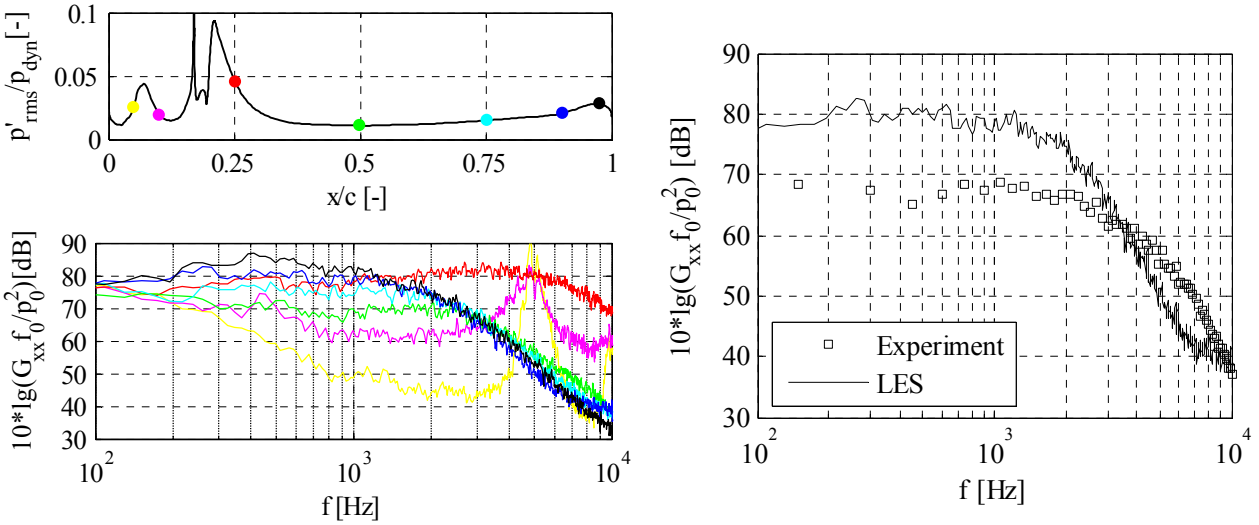

Figure 6. Upper left: LES predicted fluctuating pressure normalized with the dynamic freestream pressure (SS); lower left: surface pressure PSD at different chordwise positions indicated in the upper left figure; right: Comparison of the measured and the LES-predicted surface pressure fluctuations at $x/c = 0.9$ (SS).

3.2 Aeroacoustic Results

Fig. 7 (left) shows the measured free field sound pressure in terms of the cross spectral density level L_{Spp} of the two adjacent TE microphones M2 and M3. The airfoil sound signals were pro-

cessed according to Blake and Lynch's filtering and correlation technique. Between 300 and 3000 Hz the signal to background noise ratio is sufficiently big to identify the sound from the airfoil.

A first indicator that the dominant sound source is indeed the airfoil TE stems from the cross-correlation of microphone M2 with M1 as suggested by Brooks Pope and Marcolini. The two main peaks in the cross-correlation function in Fig. 7 (right) represent the LE and TE sound sources. The different sign and absolute values of travelling times Δt clearly indicate their location. Obviously there is a highly correlated sound source at the TE.

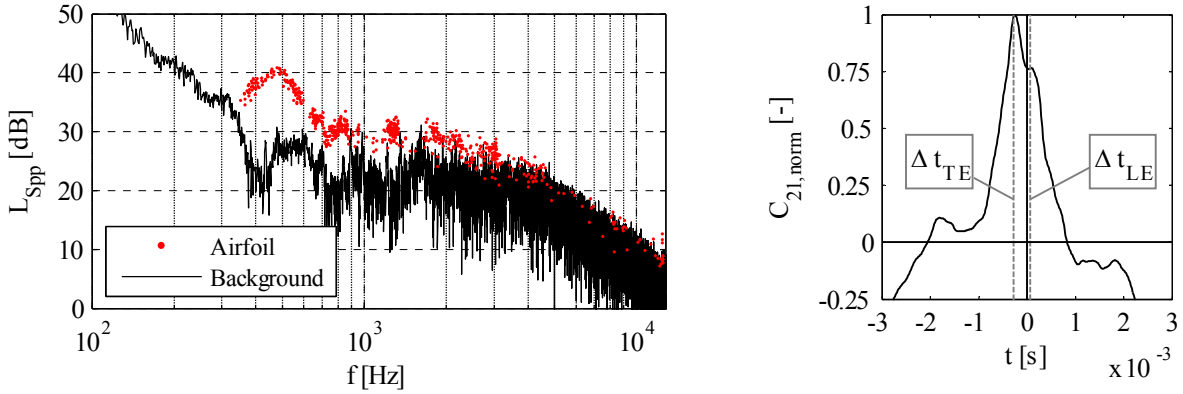

Figure 7. Left: Measured airfoil sound against background, signal processing acc. to Blake and Lynch; right: cross-correlation of TE and LE microphone (signals have been bandpassed between 100 Hz and 12.8 kHz)

A second indicator is obtained from the microphone array measurements. The sound pressure maps in Fig. 8. refer to different 1/3-octave frequency bands. In the top row two examples of the near field measurements are depicted showing the TE to be the dominant sound emitting part within a dynamic range of 6 dB. The bottom row shows measurements with the array positioned in the far-field. The data shown in the left picture were calculated using the orthogonal beamforming algorithm. Spatial resolution and dynamic range are rather poor; however, the TE can be detected as main sound source within the specified dynamic range. At higher frequencies the much more efficient Clean SC algorithm yields the best results. Here th e background noise almost drowns the sound emitted by the airfoil, but due to the large dynamic range, even here the airfoil TE can be identified as main airfoil self noise source. In general, the phased array results suggest that the largest contribution from the TE to the overall emitted sound is in the lower frequency range, which coincides with the 500 Hz hump in the spectrum of Figure 7 (left). The discussion in the following section tries to support this finding by semi-theoretical approaches.

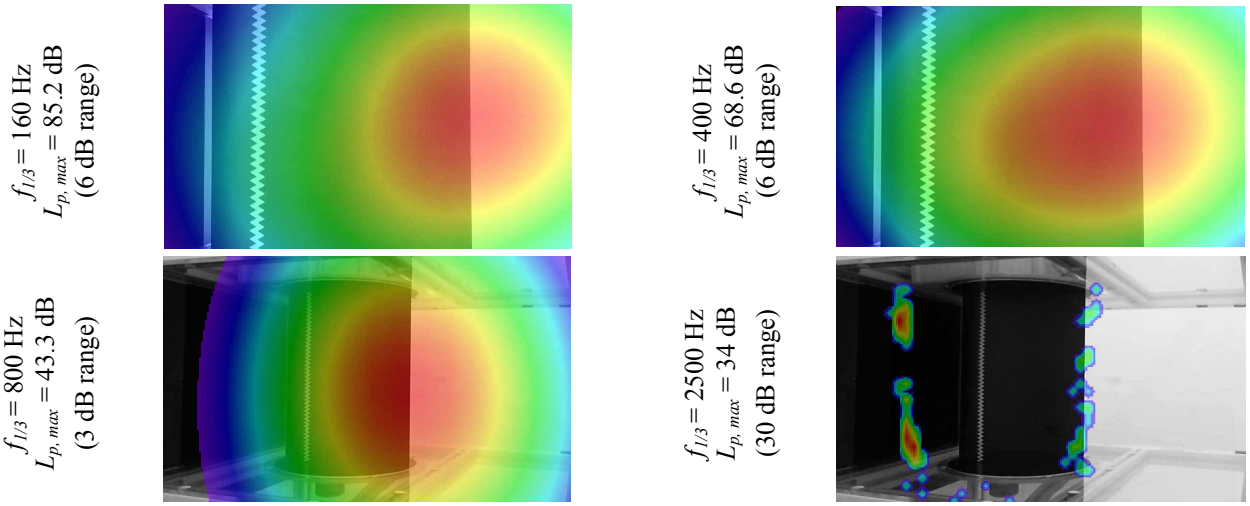

Figure 8. Microphone array measurements in the near field (top row) and far-field (bottom row), the data refer to different 1/3-octave frequency bands; different algorithms applied (view from suction side).

3.3 Further Discussion of the Acoustic Results

Numerous models for TEN-prediction are known. We employ two of them to support our experimental finding that the hump around 500 Hz in the sound spectrum of Fig. 7 (left) is indeed caused by the TE of the airfoil.

The first is the semi-empirical Brooks, Pope and Marcolini (BPM) model[1]. Basically it allows quantifying various contributors to the airfoil's overall self-noise. It is based on a set of aerodynamic and aeroacoustic measurements of a NACA 0012 airfoil blade section at varying Reynolds number and angle of attack. One has to keep in mind that the BPM-model resolves 1/3-octave frequency bands only. The self noise mechanism addressed in the present study is denoted in the BPM model as turbulent-boundary-layer trailing-edge (TBL-TE) noise. According to this model the maximum TEN emissions occur at a Strouhal-number of

$$St \equiv \frac{f\,\delta^*}{u_\infty} \approx 0.1\,. \tag{1}$$

δ^* is the boundary displacement thickness at the TE. The boundary layers of both airfoil sides are scattered at the airfoil TE and contribute independently to the overall TEN emissions. Furthermore, the TEN sound pressure level (SPL) is a function of the airfoil AOA. The overall peak TEN can be calculated as:

$$SPL_{TOT} = 10 \cdot \lg\left[10^{SPL_\alpha/10} + 10^{SPL_s/10} + 10^{SPL_p/10}\right]. \tag{2}$$

BPM then use a generalized shape function to create the TBL-TE noise spectrum. We take the AOA as α_{eff} = 4.7° and the displacement thickness from Fig. 5 (explicitly from the LES-prediction) and compare the BPM-prediction with our measurements in Fig. 9 (left). It is obvious that the BPM-predicted TEN occurs is in a similar frequency range and has a similar overall level as in our experiments. The discrepancies are most likely due to the fact that we are dealing here with a completely different airfoil S834 instead of a NACA 0012.

The second is Curle's acoustic analogy[15]. It describes sound radiation from stationary surfaces in a turbulent flow. Relevant are the forces acting from the solid surfaces on the fluid. Here, the LES-predicted fluctuating pressure at each surface element center represents the unsteady force per unit area and hence is taken as input for this prediction model. The result of Curle's prediction is presented in Fig. 9 (right) again in terms of the cross spectral density level L_{Spp} of two adjacent TE microphones. The agreement between the prediction and our experimental finding is good, even the complete hump around 500 Hz is predicted very well. The spectral levels are in the same order up to a frequency of about 1500 Hz, at higher frequencies the level is slightly underpredicted.

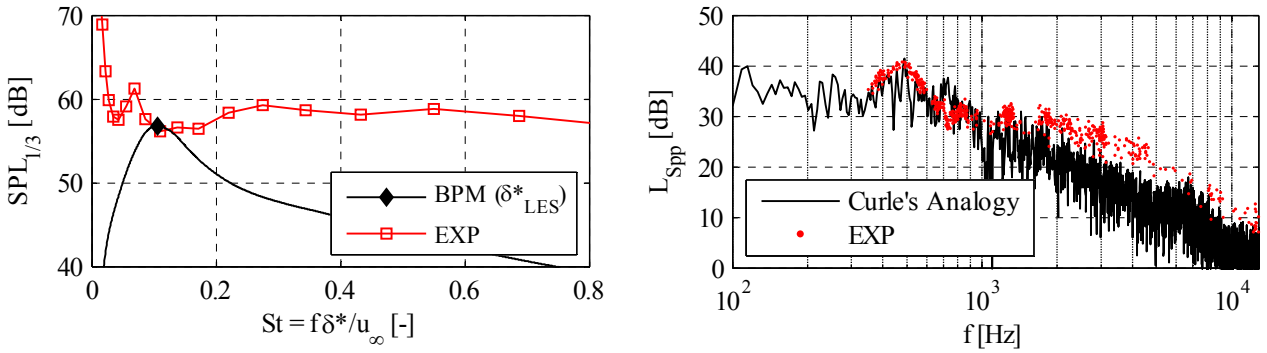

Figure 9. Comparison of a TEN prediction with experimental data for the S834 airfoil section; left: Brooks, Pope and Marcolini (BPM) model (1/3 octave bands); right: Curle's analogy (Δf_{EXP} = 1 Hz, Δf_{LES} = 5 Hz)

4. Conclusions

The TEN emission of a stationary airfoil placed in an aeroacoustic wind tunnel was investigated with advanced experimental and numerical methods. To account for high Reynolds numbers and associated boundary layer conditions appearing at full-scale wind turbine applications, the airfoil surface has been tripped at the natural transition locations corresponding to a 10-times higher Reynolds number than the prevailing Reynolds number achieved with the existing wind tunnel.

The applied boundary layer tripping was successful in so far, as it produced the targeted boundary layer parameters (e.g. displacement thickness) in the TE region of the airfoil. They are acoustically relevant for TEN. The TE of the airfoil was found to be the most dominant sound radiation region on the airfoil section. This was the result of several independent correlation techniques applied. The microphone array measurements revealed dominant contributions from the TE from 160 to at least 2500 Hz. The peak level of TEN was found at a displacement thickness based Strouhal-number of approximately 0.075, corresponding to a frequency of 500 Hz. Both sound prediction models utilized - Brooks, Pope and Marcolini (BPM) and Curle's - confirmed that the spectral hump found in the measurements is indeed attributed to the turbulent flow over the airfoil's trailing edge.

Hence, the tools applied allow a precise characterization of the airfoil TEN signature and facilitate future implementation of TEN mitigation techniques.

REFERENCES

1. Brooks, T.F., Pope, D.S., Marcolini, M.A., *Airfoil Self-Noise and Prediction*, NASA RP-1218, NASA Langely Research Center, (1989).
2. Roger, M., On the Noise from Open Rotors, in VKI Lecture Series 2006-05: Computational Aeroacoustics, Rhode-St-Genèse, Belgium, (2006).
3. Somers, D.M., *The S833, S834 and S835 Airfoils*, NREL/SR-500-36340, National Renewable Energy Laboratory, Golden Colorado, USA, (2005).
4. Oerlemans, S., Wind Tunnel Aeroacoustic Tests of Six Airfoils for Use on Small Wind Turbines, Subcontractor Report for the National Renewable Energy Laboratory (Colorado, USA), NREL/SR-500-35339, National Aerospace Laboratory NLR, (2004).
5. Winkler, J., Moreau, S., Carolus, T., Airfoil Trailing Edge Noise Prediction from Large-Eddy Simulation: Influence of Grid Resolution and Noise Model Formulation, *16th AIAA/CEAS Aeroacoustics Conference,* AIAA 2010-3704, Stockholm, Sweden, (2010).
6. Brooks, T.F., Marcolini, M.A., Pope, D.S., Airfoil Trailing Edge Flow Measurements and Comparison with Theory Incorporating Open Wind Tunnel Corrections, in *AIAA/NASA 9th Aeroacoustic Conference*, AIAA-84-2266, Williamsburg, Virginia, (1984).
7. Drela, M., XFOIL: An Analysis and Design System for Low Reynolds Number Airfoils. *Conference on Low Reynolds Number Airfoil Aerodynamics*. University of Notre Dame, (1989).
8. Mueller, T.J., In: *Fixed and Flapping Wing Aerodynamics for Micro Air Vehicle Applications*, American Institute of Aeronautics and Astronautics, USA, (2001).
9. Winkler, J., Carolus, T., Concept, Design and Characterization of a Small Aeroacoustic Wind Tunnel Facility with Application to Airfoil Measurements, *Noise Control Engineering J.*, **57** (4), (2009).
10. Determination of Sound Power Levels of Noise Sources Using Sound Pressure-Precision Methods for Anechoic and Hemi-Anechoic Rooms, International Standard ISO 3745: 2003, International Organization for Standardization, Geneva, Switzerland, (2003).
11. Blake, W. K., Lynch, D. A., Ch. 4: Source Characterization by Correlation Techniques, in *Aeroacosutic Measurements*, T. J. Mueller, ed., Experimental Fluid Mechanics, Springer-Verlag, Berlin Heidelberg New York, 218-257, (2002).
12. Sijtsma, P., Clean based on Spatial Source Coherence, *13th AIAA/CEAS Aeroacoustic Conference*, AIAA-2007-3436, Rome, Italy, (2007).
13. Menter, F., Two-Equation Eddy-Viscosity Turbulence Models for Engineering Applications, *AIAA J.*, **32**, 1598-1605, (1994).
14. Nicoud, F., Ducros, F., Subgrid-Scale Stress Modelling Based on the Square of the Velocity Gradient Tensor, *Flow, Turbulence and Combustion*, **62**, 183-200, (1999).
15. Curle, N., The Influence of Solid Boundaries Upon Aerodynamic Sound, *Proceedings of the Royal Society of London. Series A, Mathematical and Physical Sciences*, **231**, 505-514, (1955).